Molecular profiling predicts meningioma recurrence and reveals loss of DREAM complex repression in aggressive tumors

Akash J. Patel[a,b], Ying-Wooi Wan[b,c,1], Rami Al-Ouran[b,d], Jean-Pierre Revelli[b,c], Maria F. Cardenas[e], Mazen Oneissi[a,b], Liu Xi[e], Ali Jalali[a], John F. Magnotti[a], Donna M. Muzny[e], HarshaVardhan Doddapaneni[e], Sherly Sebastian[a], Kent A. Heck[f], J. Clay Goodman[f], Shankar P. Gopinath[a], Zhandong Liu[b,d], Ganesh Rao[g], Sharon E. Plon[c,d], Daniel Yoshor[a,h], David A. Wheeler[e], Huda Y. Zoghbi[b,c,d,h,i,1], and Tiemo J. Klisch[b,c,1]

[a]Department of Neurosurgery, Baylor College of Medicine, Houston, TX 77030; [b]Jan and Dan Duncan Neurological Research Institute, Texas Children's Hospital, Houston, TX 77030; [c]Department of Molecular and Human Genetics, Baylor College of Medicine, Houston, TX 77030; [d]Department of Pediatrics, Baylor College of Medicine, Houston, TX 77030; [e]Human Genome Sequencing Center, Department of Molecular and Human Genetics, Baylor College of Medicine, Houston, TX 77030; [f]Department of Pathology, Baylor College of Medicine, Houston, TX 77030; [g]Department of Neurosurgery, University of Texas MD Anderson Cancer Center, Houston, TX 77030; [h]Department of Neuroscience, Baylor College of Medicine, Houston, TX 77030; and [i]Howard Hughes Medical Institute, Baylor College of Medicine, Houston, TX 77030

Contributed by Huda Y. Zoghbi, September 6, 2019 (sent for review July 30, 2019; reviewed by Daniel A. Haber and Harold Varmus)

Meningiomas account for one-third of all primary brain tumors. Although typically benign, about 20% of meningiomas are aggressive, and despite the rigor of the current histopathological classification system there remains considerable uncertainty in predicting tumor behavior. Here, we analyzed 160 tumors from all 3 World Health Organization (WHO) grades (I through III) using clinical, gene expression, and sequencing data. Unsupervised clustering analysis identified 3 molecular types (A, B, and C) that reliably predicted recurrence. These groups did not directly correlate with the WHO grading system, which classifies more than half of the tumors in the most aggressive molecular type as benign. Transcriptional and biochemical analyses revealed that aggressive meningiomas involve loss of the repressor function of the DREAM complex, which results in cell-cycle activation; only tumors in this category tend to recur after full resection. These findings should improve our ability to predict recurrence and develop targeted treatments for these clinically challenging tumors.

NF2 | oncogenesis | brain tumor | classification | PRC2

Meningiomas are the most common primary tumors of the brain and central nervous system (1, 2), and they are most commonly benign (World Health Organization [WHO] grade I). Nevertheless, roughly 20% of meningiomas are atypical (grade II) or malignant (grade III), with a 5-y recurrence rate of up to 41% (3–5); such tumors require serial resections until they become inoperable, and the 5-y survival rate can be as low as 35% (6). At present, the WHO histopathological classification system does not consistently predict whether an individual meningioma will recur after complete surgical resection (7). We clearly need a better understanding of meningioma biology in order to develop effective complements to surgery and radiation.

There are good reasons to believe that meningioma might be amenable to the sort of molecular profiling that has transformed the diagnosis and treatment of medulloblastoma, glioma, and many other cancers in recent years (8–11). The first hint of an underlying genetic mechanism came from the observation that meningiomas frequently arise in the context of neurofibromatosis type 2 (NF2) (12). In fact, half of sporadic meningiomas and a majority of higher-grade tumors involve loss of NF2 function or loss of heterozygosity of chromosome (chr)22q, where *NF2* is located (13, 14). Several whole-exome/genome sequencing studies have identified recurrent somatic mutations in *TRAF7*, *KLF4*, *AKT1*, *SMO*, and *POLR2A* in benign (grade I) tumors (15–17). Harmancı et al. (13) found that a majority of primary atypical meningiomas have loss of *NF2* along with either genomic instability or *SMARCB1* mutations; this combination of features was not able to completely separate atypical from benign tumors, but the addition of the top 25 most differentially expressed genes raised the prediction accuracy of the model to 91% for atypical tumors with a high or medium Ki-67 index. Bi et al. (18) found that grade III tumors are less likely to have *TRAF7*, *KL4*, *AKT1*, or *SMO* mutations but more likely to show genomic instability (copy number variation). Vasudevan et al. (19) sought targetable pathways in high-grade meningiomas and found that high *FOXM1* expression is associated with poor clinical outcomes; this is one of several studies showing that DNA methylation profiles have clinical relevance (14, 19–21).

All these studies demonstrate that molecular approaches yield important insights, yet most relied on the existing WHO histopathological classification system (i.e., they studied tumors within specific WHO grades). To our knowledge, only Sahm et al. (14) studied meningiomas across all grades, using methylation arrays to

Significance

Meningiomas are the most common primary brain tumors. Although most of these tumors are benign, one-fifth will recur despite apparently complete resection. Several studies have demonstrated that genomic approaches can yield important insights into the biology of these tumors. We performed RNA sequencing and whole-exome sequencing of 160 tumors from 140 patients, which identified 3 distinct groups of meningioma that correlate with recurrence better than the current World Health Organization grading system. Our analysis also revealed that the most aggressive type was characterized by loss of the repressive DREAM complex. These findings should improve prognostication for patients and lead to viable therapeutic targets.

Author contributions: A.J.P., H.Y.Z., and T.J.K. designed research; A.J.P., J.-P.R., M.F.C., M.O., L.X., and T.J.K. performed research; D.M.M., H.D., S.S., S.P.G., G.R., and D.Y. contributed new reagents/analytic tools; A.J.P., Y.-W.W., R.A.-O., A.J., J.F.M., K.A.H., J.C.G., Z.L., D.A.W., H.Y.Z., and T.J.K. analyzed data; and A.J.P., S.E.P., H.Y.Z., and T.J.K. wrote the paper.

Reviewers: D.A.H., Massachusetts General Hospital; and H.V., Weill Cornell Medical College.

Competing interest statement: S.E.P. is a member of the Scientific Advisory Board for Baylor Genetics.

Data deposition: Raw and processed data have been deposited in the Gene Expression Omnibus (GEO) database, https://www.ncbi.nlm.nih.gov/geo (accession no. GSE136661).

[1]To whom correspondence may be addressed. Email: yingwoow@bcm.edu, hzoghbi@bcm.edu, or klisch@bcm.edu.

This article contains supporting information online at www.pnas.org/lookup/suppl/doi:10.1073/pnas.1912858116/-/DCSupplemental.

First published October 7, 2019.

find 2 major epigenetic groups with 6 subclasses between them. Given that global epigenetic changes are just one mechanism by which cells alter expression of large groups of genes, we decided to focus on transcriptional profiling. This approach has the advantage of yielding functional biological information about tumor behavior. We therefore used an unsupervised approach to analyze RNA sequencing (RNA-seq) and whole-exome sequencing (WES) data from 160 fresh-frozen grade I, II, and III meningioma samples. Our analysis yielded 3 distinct types of meningioma that correlate with clinical outcomes better than the WHO classification; it also revealed a molecular signature for the most aggressive tumors that provides biological insight into their etiology.

Results

Patient Demographics and Pathologic Characteristics. We analyzed 160 meningioma samples from 140 patients (see *Methods* for details). According to the WHO histopathological classification system for meningioma, 121 tumors were grade I (benign), 32 were grade II (atypical), and 7 were grade III (malignant). Female sex confers greater risk for meningioma (1), and our cohort reflected the expected proportions, with 90 (64%) female and 50 (36%) male subjects. The median age at the time of initial surgery for these patients was 60 y (range 21 to 81 y). Seventy-nine percent of patients underwent a gross total resection, 22% underwent a subtotal resection, and in one case the extent of resection was unknown. The follow-up period ranged from 0 to 91 mo (median 28 mo). Twenty-four tumors (17%) had a local recurrence. The recurrence rate for WHO I grade tumors was 11%, for grade II 42%, and for grade III 83%. The patient characteristics and pathology of our cohort are presented in Dataset S1. None of the tumors in our discovery or independent validation set had been treated with adjuvant radiation prior to profiling. Five patients had had radiation as children (4 for cancers and 1 for tinea capitis); these are marked with an asterisk in Dataset S1.

Identification of Meningioma Subtypes by Transcriptome Analysis. To determine whether meningiomas could be differentiated based on gene expression profiles, we used principal component analysis (PCA) on a discovery set of 97 tumors [77 WHO grade I and 20 WHO grade II; of note, we had no primary grade III tumors, which are exceedingly rare as they are usually recurrences (22)]. The tumors did not cluster into distinct groups based on WHO grade (Fig. 1*A*).

We then employed nonnegative matrix factorization (NMF) clustering for k = 2 to k = 7 using the 1,500 genes that varied most among the tumor samples. NMF is an unsupervised machine-learning approach commonly used for cancer subtypes discovery (8). After 1,000 iterations, 3 clusters (k = 3) emerged as providing the best fit as determined by the consensus membership, cophenetic, and silhouette scores (Fig. 1*B* and *SI Appendix*, Fig. S1 *A–C*). We evaluated the cluster significance of the 3 subtypes using SigClust (23) and observed statistical significance between cluster

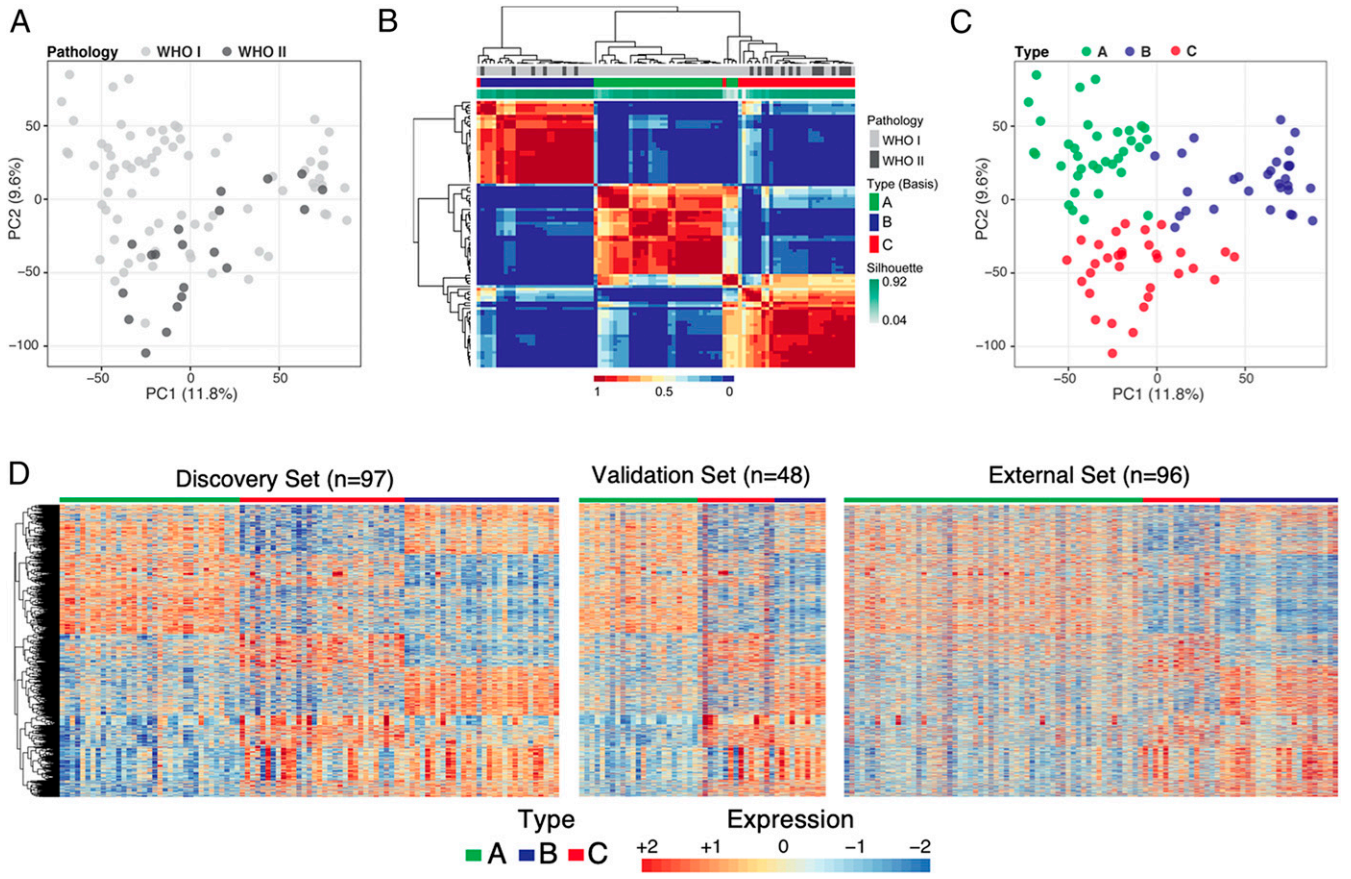

Fig. 1. Identification of meningioma subtypes using gene expression profiles. (*A*) PCA on all genes of 97 tumors colored by WHO grading. WHO grade I tumors are represented by light gray circles; WHO grade II tumors are represented by dark gray circles. (*B*) Consensus matrix of the tumors for k = 3 from 1,000 runs of NMF analysis depicts 3 distinguishable types based on the gene expression data. (*C*) PCA on all genes, colored according to molecularly defined types. (*D*) Expression heat map of the 3,484 genes common in all 3 datasets. The expression patterns of these genes distinguish 3 expression types in our discovery set (*Left*), validation set (*Middle*), and publicly available dataset (*Right*). Type A is labeled in green, type B in blue, and type C in red. Labels in the 2 independent validated sets were predicted using a random forest trained on discovery set.

boundaries (*SI Appendix*, Fig. S1*D*). The 3 clusters can also be discerned from the expression heat map (*SI Appendix*, Fig. S1*E*) and exhibit significant differences in WHO grade representation (compare Fig. 1 *A* and *C*; $P = 0.0020$, ANOVA): A (green) is populated exclusively with WHO grade I tumors, B (blue) contains mostly WHO grade I (79%) tumors, with 21% grade II, and C (red) contains similar proportions of WHO grade I and II tumors (56% and 44%, respectively; Dataset S1). Because the WHO grade III tumors in our cohort were all recurrences, they were not included in the primary transcriptome analysis.

To understand the robustness of the 3 molecular subtypes, we examined the gene expression profiles associated with each cluster in 2 independent datasets: an independent cohort of 48 tumors (39 WHO grade I and 9 WHO grade II) and a published microarray dataset of 96 meningiomas (16). Since the 3 datasets were profiled on 2 different platforms, we first filtered out genes that are not expressed in any tumors across the 3 datasets. Then, on the discovery dataset, we performed pairwise comparisons between each cluster to identify genes that are differentially expressed with a minimum absolute fold change of 1.5 and a false discovery rate of 1%. This yielded 3,484 genes, which we used to build a random forest classifier to predict a cluster label of each sample. The random forest was trained on the discovery dataset of 97 samples. To avoid overfitting due to small sample size, we evaluated the fitted model in 2 independent validation datasets which were never used for feature selection or training of our random forest classifier. We observed concordant gene expression patterns for all 3 clusters across training and validation sets (Fig. 1*D*). These results provide evidence that the molecular types designated by differential gene expression of our discovery set are stable, even across platforms.

We next analyzed the association of clinical variables with the 3 transcriptionally defined types (from here we will refer to our 3 molecular classes as types A, B, and C, as distinct from the WHO classification system's grades I, II, and III). One important clinical variable is the MIB1 index, a measure of the mitotic activity of the tumor, which has prognostic significance (24). The median MIB1 index tracked with molecular type, being lowest in type A, intermediate in type B, and highest in type C (2.5, 3.5, and 6.3, respectively; Fig. 2 *A*, *Upper*, $P = 0.0026$, ANOVA), despite 56% of our type C tumors' being classified as WHO grade I. While the sample size is smaller in our validation cohort, we observed the same trend (Fig. 2 *A*, *Lower*). To ensure that these differences were not due to a mixture of WHO grade tumors in the types, we analyzed the MIB1 index of only the WHO grade I tumors (Fig. 2 *B*, *Left*) and only the grade II tumors (Fig. 2 *B*, *Right*) and found the same tracking of MIB1 index from molecular types A to C, within each WHO grade. Because the MIB1 index is based on Ki-67 immunohistochemistry staining, which is subject to interobserver variability (25, 26), we quantified its average transcript levels (MKI67) and observed a concordant result: statistically significant increases from molecular types A to C in our discovery cohort (*SI Appendix*, Fig. S2 *A*, *Upper*; $P < 0.0001$) and an identical trend in our validation cohort (*SI Appendix*, Fig. S2 *A*, *Lower*).

It has been reported that tumors with different somatic mutations cluster to different intracranial regions (e.g., TRAF7 and SMO mutant tumors tend to form in the anterior skull base) (15). We therefore asked whether any of our 3 molecularly defined types were associated with specific locations (Fig. 2*C* and Dataset S1). Although the sample size relative to the number of factors precludes making strong conclusions, we used a generalized linear model (Poisson link function) analysis to compare the distribution of tumors for each type across 16 anatomical locations. Only the anterior skull base and occipital locations showed a significant difference between types (adjusted $P = 0.0004$ and 0.0329, respectively), with type A tumors more likely to be located in the anterior skull base and type C tumors more likely to arise in the occipital region (Fig. 2*C*). We next compared the spatial distribution of tumor types between datasets (Bayesian information criterion comparison); we found no significant interactions with datasets (discovery vs. validation), suggesting these patterns were consistent in both samples.

We also examined the sex distribution in our expression types. In our discovery set, types A and B show the expected 2:1 female-to-male distribution, but 56% of patients in type C are male ($P = 0.0240$; Dataset S1).

Finally, we assessed the recurrence-free survival (RFS) across the 3 types (Fig. 3). We did not analyze overall survival because only 3 patients died (1 in the discovery set and 2 in our validation set). We first analyzed our discovery set of 97 tumors. WHO grade II tumors tended to have a shorter RFS than WHO grade I tumors, but this trend did not quite reach significance (Fig. 3 *A*, *Left*; log-rank $P = 0.0490$). On the other hand, our type A and B tumors had an indistinguishably long RFS with only 4 recurrences, even though 21% of the type B tumors would be classified by the current WHO system as "high-grade." Type C tumors, however, have a significantly shorter RFS than the 2 other types (Fig. 3 *A*, *Right*; log-rank $P = 0.0006$), despite the fact that the majority of the tumors in type C are classified as WHO grade I.

To ensure that the extent of resection was not responsible for these RFS differences, we looked at RFS for only those tumors that underwent gross-total resection. Both WHO grade I and II had recurrences, with more for WHO grade II (Fig. 3 *B*, *Left*, log-rank $P = 0.0180$), but of our molecularly defined types only type C tumors recurred (Fig. 3 *B*, *Right*, log-rank $P = 0.0002$).

To rule out the effect of WHO grade on the recurrence trends seen with our types, we analyzed the RFS of our types within each WHO grade in our discovery cohort (similar to our MIB1 analysis). We found that type C WHO grade I tumors have much worse recurrence rates (33%) than type A (8.6%) or type B (4.2%) WHO grade I tumors or WHO grade I tumors as a whole (13%) (Fig. 3 *C*, *Left*; log-rank $P = 0.0160$, ANOVA). The same holds true within WHO grade II tumors (Fig. 3 *C*, *Right*; log-rank $P = 0.0900$, ANOVA): Type C WHO grade II tumors have a 57% recurrence rate, higher than type B (16.7% recurrence rate) or all WHO grade II tumors (45% recurrence rate).

Thus, our expression-based classification identifies WHO grade I/II tumors that have a high risk of recurrence. These data also suggest that total resection is less likely to cure type C tumors.

Copy Number and Somatic Alterations in Meningiomas. Since high-grade meningiomas have more chromosomal abnormalities (13, 18), we analyzed the 3 types of tumors for genomic instability using copy number data derived from WES (Fig. 4). We had copy number data for 84 tumors in the discovery cohort and 44 in the validation cohort. Type A had no notable chromosomal losses or gains. Type B tumors showed significant loss of chr22q, the most commonly reported chromosomal abnormality in meningioma (27) (Fig. 4*A*; 84%; $P < 0.0001$, χ^2). Type C manifested the most genomic instability, showing loss of chr22q (89%; $P < 0.0001$ χ^2) and chr1p (79%; $P < 0.0001$, χ^2), the second most common reported abnormality (27, 28). Furthermore, over 20% of the type C tumors showed losses in chr3p, chr4p, chr6q, chr14p, chr14q, or chr18q (Fig. 4 *A*, *Upper*). Both validation sets replicated these results (Fig. 4 *A*, *Lower*). Interestingly, the type of chromosome loss is almost sufficient to distinguish between types. Combining all datasets, retaining both chr1p and chr22q identified type A tumors with a 94% sensitivity and 86% specificity with a positive predictive value (PPV) of 86% and a negative predictive value (NPV) of 94%. Deletion of only chr22q identified type B with a sensitivity of 76%, specificity of 95%, PPV of 83%, and NPV of 92%. Deletion of both chr22q and chr1p identified type C with a sensitivity of 68%, specificity of 95%, PPV of 83%, and NPV of 90%. We also examined the distribution of chromosome loss by sex and did not find a significant difference between females and males (Fig. 4*B*). However, we noticed that the ratio of female to male differed between types: Combining all

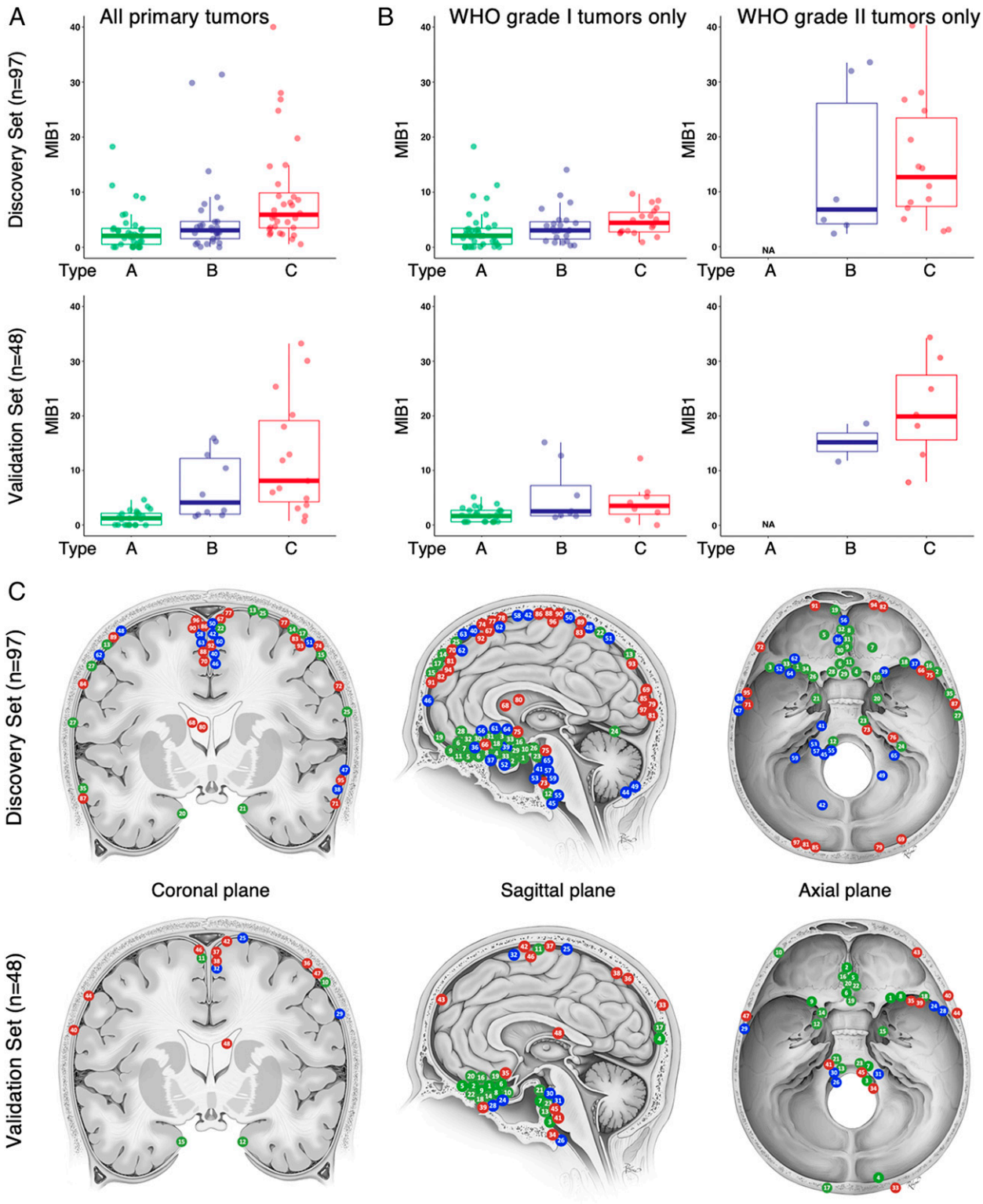

Fig. 2. Clinical characteristics of gene expression-defined meningioma types. Type A is labeled in green, type B in blue, and type C in red. (*A*) Boxplots showing the median MIB1 index for types A to C in the discovery set ($P = 0.0026$, ANOVA, *Upper*) and the validation set ($P < 0.0001$, ANOVA, *Lower*). (*B*) Boxplot of the MIB1 for types A to C for only WHO grade I tumors (*Left*) in the discovery set ($P = 0.4359$, ANOVA, *Upper*) and the validation set ($P = 0.0044$, ANOVA, *Lower*) and WHO grade II tumors (*Right*) in the discovery set ($P = 0.6059$, ANOVA, *Upper*) and the validation set ($P = 0.3380$, ANOVA, *Lower*). (*C*) Location of tumors in our cohort in the discovery set (*Upper*) and validation set (*Lower*). Each tumor is marked on 2 views, either coronal and sagittal or axial and sagittal, respectively (Dataset S1). Image created by Katherine Relyea and printed with permission from Baylor College of Medicine.

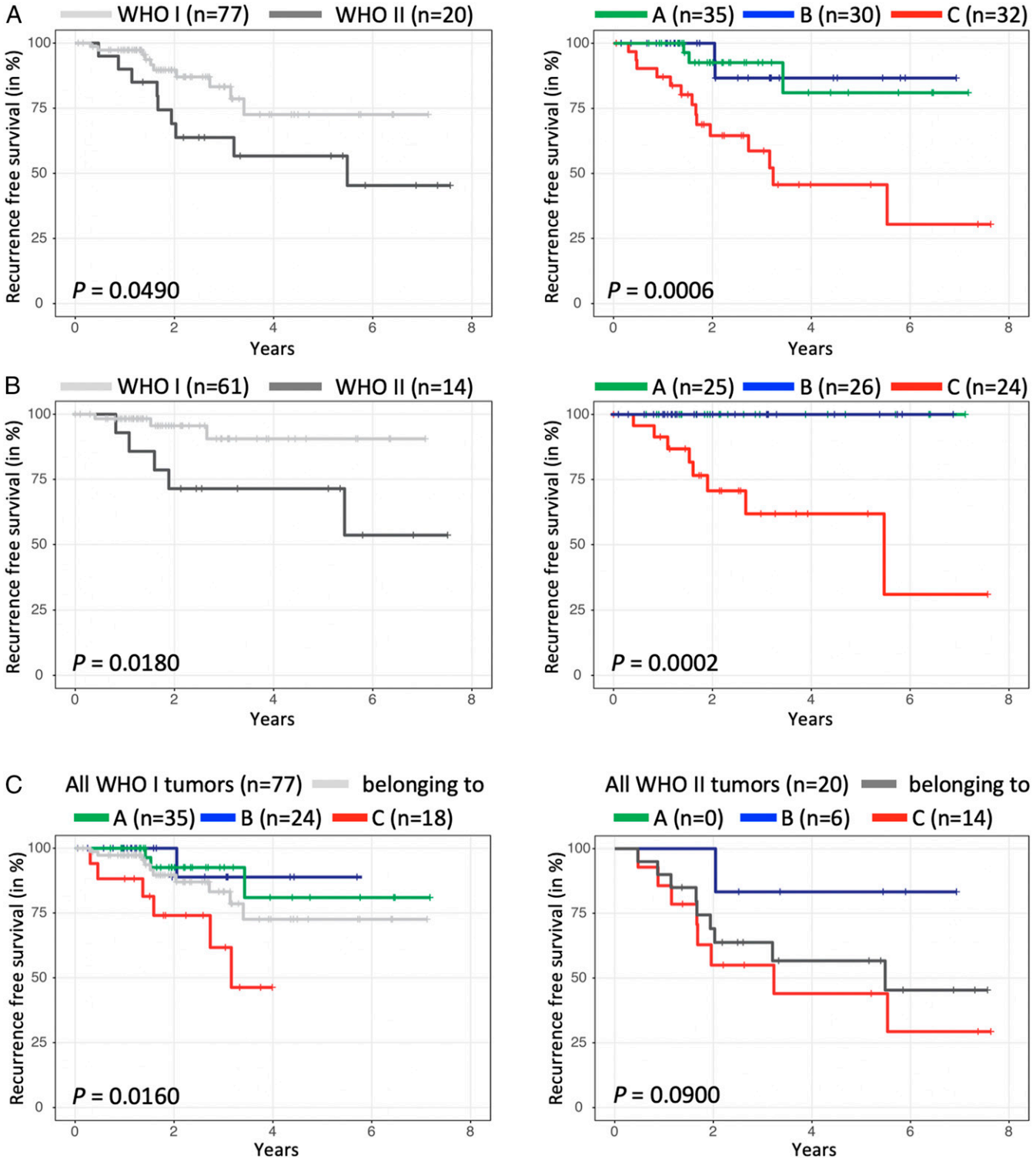

Fig. 3. RFS of WHO grade and gene expression-defined meningioma types. RFS analysis based on (*A*) WHO grading (*Left*) and by expression-defined types (*Right*) in all tumors and (*B*) only tumors that underwent complete resection. (*C*) RFS for expression-defined types within only WHO grade I tumors (*Left*) or WHO grade II tumors (*Right*) shows the ability of the molecular typology to refine RFS despite WHO grading. n represents the initial number of tumors for each curve.

datasets, type A has 78% female patients, type B has 77%, and type C has only 51% ($P = 0.0008$, χ^2).

Given that the tumor types could nearly be distinguished based on copy number data alone, we calculated the PPV and NPV for recurrence based on copy number alterations. Loss of both chr22q and chr1p predicted recurrence with a sensitivity of 75%, specificity of 78%, PPV of 44%, and NPV of 93%. For tumors that underwent complete resection in our cohort, loss of both chr22q and chr1p predicted recurrence with a sensitivity of 100%, specificity of 76%, PPV of 36%, and NPV of 100%.

WES also revealed 3,094 somatic mutations in our discovery cohort with a median of 0.47 mutations per megabase, which did

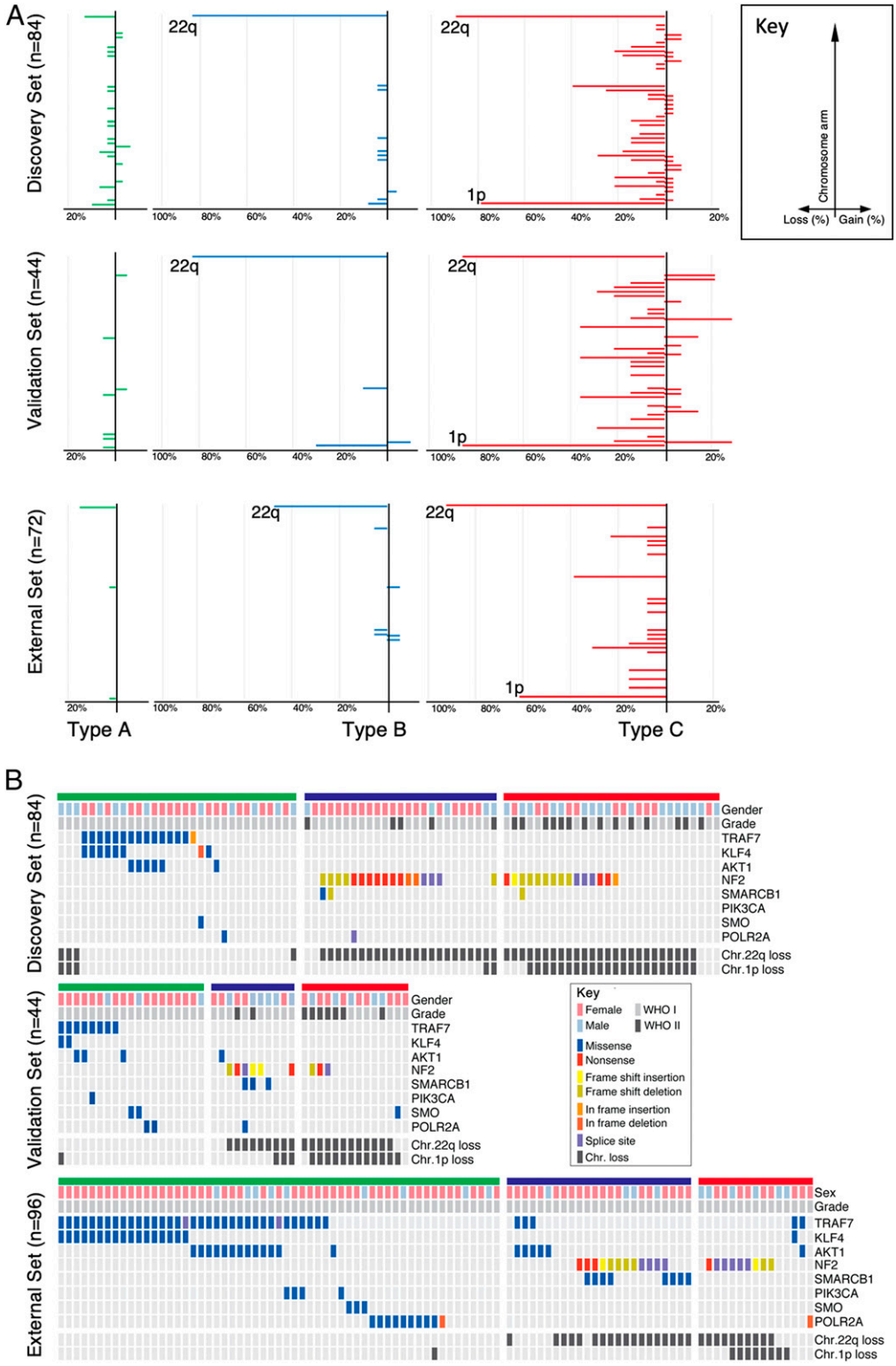

Fig. 4. Genomic landscape of meningiomas by gene expression-defined types. Type A is labeled in green, type B in blue, and type C in red. (*A*) Differences in chromosomal alterations by type are shown with losses to the left and gains to the right. (*B*) Oncoprint depicting the mutation profiles of each meningioma type in the discovery set (*Upper*) the internal (*Middle*) and external validation set (*Lower*).

not differ between tumor types (type A, 0.44; type B, 0.40; type C, 0.52; $P = 0.4951$). Specific mutations did, however, cluster according to type. Only type A tumors contained mutations in *TRAF7* (Fig. 4*B*; 43%, 40%, and 61% in the discovery, validation, and external set, respectively). Type A also contained the highest percentage of *KLF4* (26%, 10%, and 30%) and *AKT1* (19%, 15%, and 23%) mutations (Fig. 4*B*). In contrast, NF2 mutations were seen only in types B (68%, 50%, and 50%) and C (54%, 21%, and

60%). These mutations were usually combined with a loss of the other allele on chr22p. SMARCB1 mutations were primarily seen in type B, especially in the external set. *TERT* promoter mutations have been found in 13% of meningiomas and portend a worse prognosis (29–31). In both our discovery and validation set there were 108 tumors whose sequencing included the *TERT* promoter. Of these, 13 tumors had a mutation in the *TERT* promoter, but they fell into all 3 tumor types (Dataset S1; $P = 0.7623$, χ^2).

As the prevalence of NF2 mutations did not differ between types B and C (68% and 54%, respectively; $P = 0.2837$, χ^2), we next explored whether the degree of NF2 expression loss could distinguish tumors in these types. Both types have markedly reduced levels of NF2 expression compared to type A (*SI Appendix*, Fig. S2*B*; $P < 0.0001$) but did not differ from one another in this regard (*SI Appendix*, Fig. S2*B*; $P = 0.1400$). Both showed typical loss of function variants (nonsense and frameshift) spanning the NF2 coding region (Fig. 4*B* and Dataset S2).

In sum, type A is characterized by recurrent somatic mutations in *TRAF7*, *KLF4*, and *AKT1* but lacks any significant chromosomal gains/losses. Type B is characterized primarily by mutation in NF2 and loss of chr22q, and type C meningiomas have a significant burden of chromosomal gains/losses, most commonly loss of chr22q and chr1p together. Like WHO grade II and III tumors (22), our type C has a roughly equal proportion of females and males.

Gene Set Enrichment Analysis Further Distinguishes Types B and C. To better differentiate types B and C and understand the biological pathways underlying these transcriptional changes, we performed gene set enrichment analysis (GSEA) (32, 33) for each expression type using the genes highly expressed in that type (Dataset S3). No single underlying pathway emerged for type A (Dataset S4). Four out of the 5 enriched categories in type B suggest that these tumors have lost the repressive activity of the PRC2 methyltransferase complex (Dataset S4). Genes highly overexpressed only in type C clustered in cell-cycle modules, especially the G2/M checkpoint, which is regulated by the repressive transcription factors of the E2F family, such as E2F4, and its associated repressor, the DREAM complex (34). The 2 modules "genes with promoters bound by E2F4" and "targets of the DREAM complex" were the most enriched modules (Dataset S4).

To determine whether these 2 repressor complexes truly reflect biological differences between these tumor types, we evaluated the enrichment scores of their target genes in all 3 types (Fig. 5*A*). Strikingly, type B is characterized by the loss or dysfunction of the repressive PRC2 complex, whereas type C is characterized by loss or dysfunction of the repressive DREAM complex.

Loss of the PRC2 Complex in Type B. The PRC2 complex is responsible for H3K27 di- and trimethylation and subsequent chromatin silencing. The core subunit consists of EED, SUZ12, and EZH1 or EZH2. We hypothesized that this complex is not forming or functioning in type B tumors, resulting in up-regulation of the PRC2 target genes, as identified by the unbiased expression clustering. Therefore, we used cellular lysates from 5 tumors of each type and immunoprecipitated the PRC2 complex using EZH1 (Fig. 5*B*). All tested proteins were expressed in all tumors (Fig. 5*B*, lysate lanes). Both EED and SUZ12 were detected in the EZH1 immunoprecipitates of type A and C tumors, but not type B tumors. This strongly suggests that the core complex is formed in type A and C tumors but not in type B tumors. Consistent with this finding, the PRC2 complex's direct targets, the HOX transcription factors (35, 36), were significantly enriched only in type B (Fig. 5*C*; q value < 0.0001).

To clarify whether loss of the PRC2 complex underlies the transcriptional dysregulation seen in type B, we transfected 293T cells with either wild-type EZH1 (amino acids 1 through 747) or SET domain–depleted EZH1 (37) (EZH1-ΔSET, amino acids 1 through 512; Fig. 5*D*). The SET domain of EZH1 is responsible for the lysine-specific histone methyltransferase activity: Without this domain, PRC2 cannot perform H3K27 methylation, and so it enables aberrant gene activation (38, 39). After 48 h of overexpression, we performed qRT-PCR analysis of 15 genes that were all significantly up-regulated in type B. We chose to include known PRC2 target genes (RBP4, ELN, CTGF, SFRP4, EPHB3, and ATOH8) (40), including those which are also homeobox genes (NKX6.1, HOXB2, and MKX) (40) (Dataset S3). We found all except one of these genes significantly up-regulated in cells overexpressing EZH1-ΔSET compared to wild-type EZH1 (Fig. 5*D*). Because meningiomas are thought to arise from arachnoid cap cells, we also generated an immortalized cell line from arachnoid cells (see *Methods* for cell line establishment). As with the 293T cell line, the tested genes were up-regulated upon loss of PRC2 complex function (Fig. 5*D*).

In sum, type B meningioma appear to have lost PRC2 complex function.

Loss of the DREAM Complex in Type C. The DREAM complex is a highly conserved master regulator of the cell cycle (34). It consists of MuvB core proteins: LIN52, LIN9, LIN37, LIN54, and RBBP4. When this core is bound to RB-like proteins (RBL1/2) and E2F, it forms the repressive DREAM complex, which keeps the cell quiescent. When the core associates with MYBL2 and FOXM1, however, it forms the activating DREAM complex, which allows cell-cycle progression and subsequent proliferation. Interestingly, tumors from type C had the highest proliferation index, and a recent study found elevated expression of FOXM1 associated with high-grade meningiomas (13, 19).

We found increased expression of both FOXM1 and MYBL2 in our type C tumors, which aligns with our previous results suggesting that the DREAM complex has lost its repressive activity and allowed up-regulation of these 2 target genes. To confirm that type B and type C tumors differ in the form of the DREAM complex that they express, we immunoprecipitated the core complex in tumors from all 3 types using LIN37. All investigated proteins were expressed in all tumors (Fig. 5*B*, lysate lanes), but RBL2 was associated with the core only in type A and B tumors (Fig. 5*B*). On the other hand, only in type C tumors was the core associated with both FOXM1 and MYBL2. Thus types A and B contain the repressive form of the DREAM complex, whereas type C tumors contain the activator forms of the complex.

If this is indeed the case, we would expect to see increased expression of DREAM target genes in type C tumors and decreased levels in the other 2 types. GSEA revealed that known DREAM target genes are highly enriched only in type C tumors (Fig. 5*C*; q value < 0.0001). Using a strategy similar to that used for type B and the PRC2 complex, we took advantage of recently published dominant-negative forms of 2 MuvB core members, LIN37 (41) and LIN52 (42). It has been shown that mutations in 2 small domains in LIN37 (CD1 and CD2) result in the loss of the repressive function of the DREAM complex (LIN37-WT [amino acids 1 through 243] and LIN37-DN) (41), and inhibiting phosphorylation of serine28 on LIN52 results in similar phenotypes (LIN52-WT [1 through 116] and LIN52-DN) (42). We performed qRT-PCR analysis of 14 genes that were all significantly up-regulated in type C, only some of which were known DREAM targets (MYBL2, FOXM1, TTK, PBK, MELK, and CDK1) (43). Overexpression of both dominant-negative constructs resulted in the up-regulation of these genes in both 293T cells (Fig. 5*D*) and our arachnoid cell line (Fig. 5*D*).

In sum, type C meningiomas appear to be characterized by loss of the repressive DREAM complex function.

Recurrent Tumors Match the Gene Expression Profile of the Original Tumor. Nine patients in our cohort had at least one resected recurrence with tissue available; 2 of these patients had multiple recurrences. Tumor progression was seen in 3 patients with type A

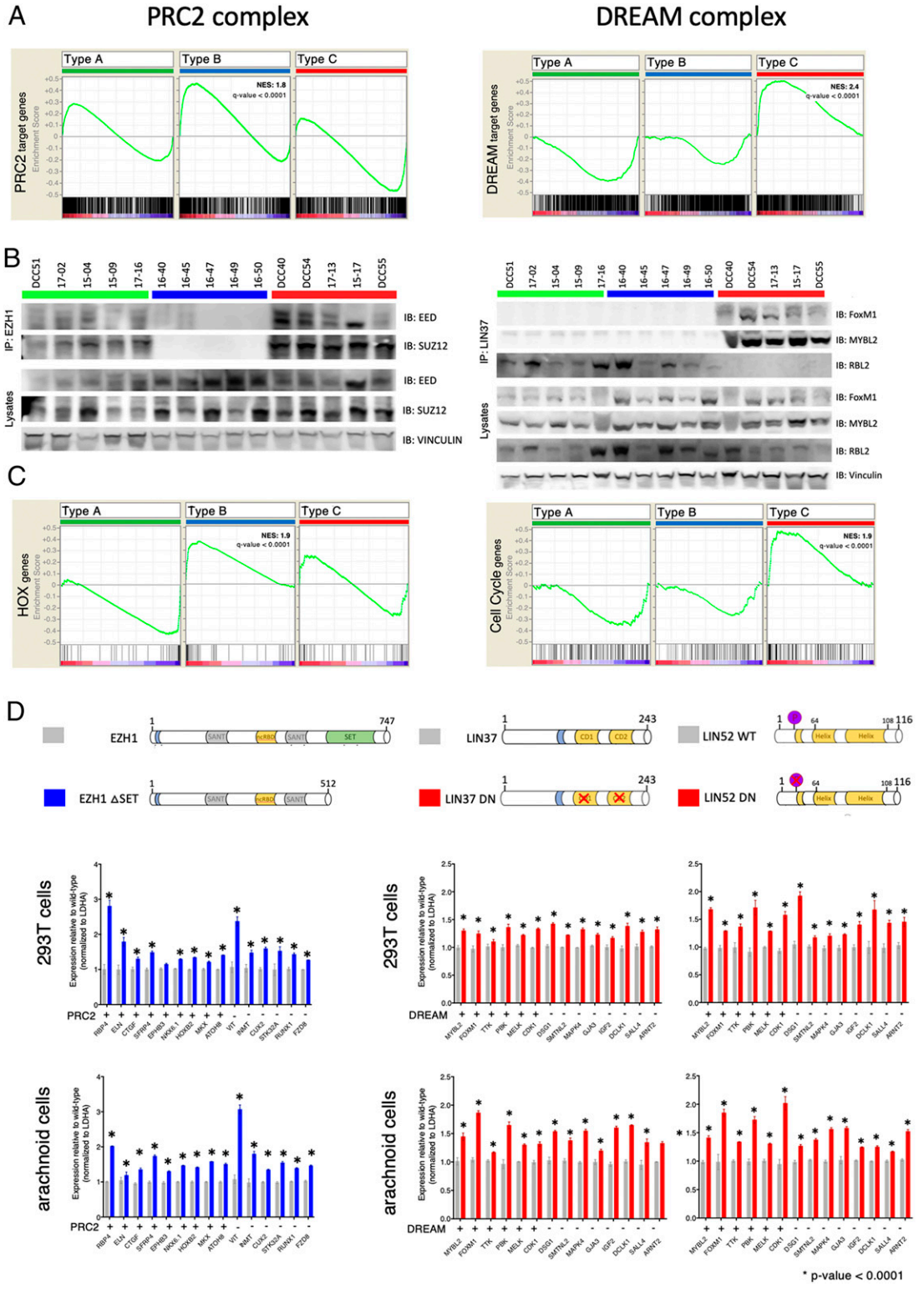

Fig. 5. Validation of PRC2 and DREAM complex disruption in type B and C tumors, respectively. (*A*) GSEA analysis of the PRC2 (*Left*) and DREAM (*Right*) target genes from each type. (*B*, *Left*) Coimmunoprecipitation studies using 5 tumors per type for EZH1 then probed for anti-EED and anti-SUZ12. (*B*, *Right*) Coimmunoprecipitation studies using 5 tumors per type for LIN37 then probed for anti-FoxM1, anti-MYBL2, and anti-RBL2. (*C*) GSEA analysis shows that HOX genes are enriched in type B (*Left*) and cell-cycle genes in type C (*Right*). (*D*) qRT-PCR analysis measuring expression levels of type-specific up-regulated genes and in 293T and arachnoid cells. (*Left*) Cells were transfected with either wild-type hEZH1 or hEZH1 ΔSET (dominant-negative EZH1). (*Right*) Cells were transfected with either wild-type hLIN37 or dominant-negative hLIN37 (left side) or either wild-type hLIN52 or dominant-negative hLIN52 (right side).

tumors who could not have a complete resection due to tumor location. Gene expression profiling of these recurrent tumors demonstrated that they all remained within the type of the original tumor (Fig. 6 and Dataset S1). Interestingly, 3 patients started with WHO grade II tumors that progressed to WHO grade III tumors, but their transcriptomic classification nonetheless remained the same (type C). Similarly, 3 patients with WHO grade I tumors had inexplicably rapid recurrences, despite complete resection in one; both their primary and recurrent tumors were type C. Of note, one recent study showed that a single grade III meningioma can be genetically heterogeneous (31); while we did not transcriptionally profile different parts of a tumor, this is something to be considered in future studies. Nevertheless, the consistency of the recurrent tumor profiles with that of their primary tumors suggests that the type C classification remains stable over time.

Discussion

The current histopathologic system for classifying meningiomas has shown some ability to predict clinical course, with WHO grade II and III tumors generally tending to recur. However, a substantial number of grade I tumors also recur, despite successful resection and apparently benign features. Here we used unsupervised gene expression clustering of RNA-seq data from a large cohort of meningioma tumors to define new types that better correlate with RFS and proliferation as measured by the MIB1 index. Most importantly, our expression-based model identifies tumors that are at high risk for recurrence, including those that would be classified as WHO grade I. For example, one of the patients in our clinic whose tumors are profiled in this study had total resection of a grade I tumor that recurred 2 y later; complete resection of this second tumor, also grade I, was insufficient to prevent a second recurrence 18 mo later—still grade I, although the MIB1 index had risen to 9.1. Our molecular classification, however, identified all of the tumors in this patient as type C.

A major difference between our study and previous explorations of the genomic landscape of meningioma is that those studies maintained the framework of the existing WHO histopathological classification for their molecular analysis (13, 15–19, 44). For example, one study of atypical (grade II) tumors found the majority to have NF2/chr22q loss and genomic instability along with overexpression of the E2F2 and FOXM1 transcriptional networks (13). Another study of high-grade tumors found overexpression of FOXM1 to be associated with poor clinical outcome (19). Only by analyzing both low- and high-grade tumors in our cohort were we able to distinguish the different biology of type B and C tumors.

There are 2 limitations to our study. Several previous studies have explored DNA methylation profiling (14, 19–21), and it would be ideal to compare our classification system with that proposed by Sahm et al. (14) by performing RNA-seq and methylation profiling on the same samples. [Methylation and expression may (45) or may not (46) correlate.] Unfortunately, the data in these papers are not publicly available, and thus could not be compared. The second limitation is the relatively short median follow-up of 28 mo for tumors with a typically indolent course. Even so, our RFS data were sufficient to identify an aggressive type of meningioma that would otherwise be classified as WHO grade I.

Salient Features of Types A, B, and C. In our cohort, type A tumors were characterized by mutations in *TRAF7*, *KLF4*, and *AKT*, which confirms previous observations in benign meningiomas (15, 17). It is possible that the downstream consequences of these mutations converge biologically.

In our type B tumors, 91% showed loss of chr22q. Our data suggest that these tumors lose PRC2 complex function and recur as infrequently as type A tumors. (A handful of type A tumors also had chr22q loss, but the number was only within the expected error rate based on the size of our discovery cohort.) Our current data suggest that if type A and B tumors are completely resected they do not recur.

Type C tumors were instead characterized by the activator forms of the DREAM complex and subsequent up-regulation of its target genes, including MYBL2 and FOXM1. Elevated FOXM1 levels were recently reported in aggressive meningiomas (19) [as well as other cancers (34)], but our findings suggest that this up-regulation is secondary to the loss of DREAM complex-mediated repression. Our findings suggest that FOXM1 and MYBL2 act as coactivators of the DREAM complex rather than as independent transcription factors.

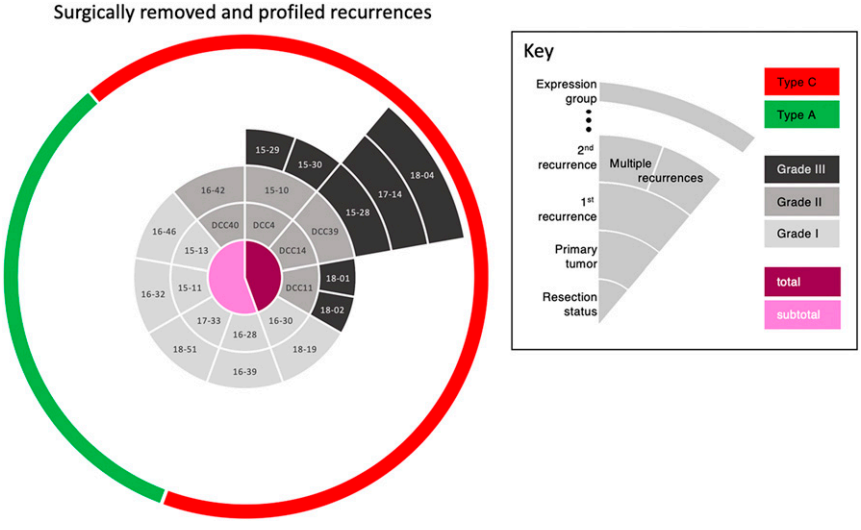

Fig. 6. Timeline of tumor recurrences by patient. The central circle indicates whether the resection of the primary tumor was partial (pink) or total (magenta). The second circle identifies the primary tumor by ID number (light gray represents WHO grade I; medium gray is grade II). The third circle identifies the first recurrence, with tone of gray indicating the WHO grade. The remaining segments, all dark gray (grade III), indicate further recurrences over time. The green and red in the rim of the circle denote types A and C, respectively. Strikingly, whereas the WHO classification changes from primary tumor to recurrence in many cases (different shades of gray), the transcriptomic type classification did not—a primary tumor of type C remained type C throughout all recurrences.

Table 1. Clinical features of patients and their primary meningiomas

Characteristic	Discovery set					Validation set			
	All tumors (n = 97)	Type A (n = 35)	Type B (n = 30)	Type C (n = 32)	P value between types	All tumors (n = 48)	Type A (n = 23)	Type B (n = 10)	Type C (n = 15)
Sex, no. of patients (%)									
Male	36 (38)	12 (34)	7 (23)	18 (56)	**0.0240**	14 (30)	3 (13)	6 (60)	6 (40)
Female	60 (62)	23 (66)	23 (77)	14 (44)		32 (70)	20 (87)	4 (40)	9 (60)
Median age, y at surgery (range)	60 (27–81)	62 (33–79)	58.5 (27–81)	58.5 (33–78)	0.465	59 (18–81)	58 (21–78)	63.5 (26–81)	63 (18–77)
Location (%)									
Anterior cranial fossa	15 (16)	13 (37)	2 (7)	0 (0)	**0.0001**	7 (15)	7 (30)	0 (0)	0 (0)
Middle cranial fossa	2 (2)	2 (6)	0 (0)	0 (0)	0.1930	2 (4)	2 (9)	0 (0)	0 (0)
Sphenoid wing	16 (16)	9 (26)	5 (17)	2 (6)	0.1930	9 (19)	5 (22)	2 (20)	2 (13)
Parafalcine	15 (15)	1 (3)	7 (23)	7 (22)	0.1800	6 (13)	1 (4)	1 (10)	4 (27)
Petroclival	7 (7)	1 (3)	5 (17)	1 (3)	0.1930	2 (4)	2 (9)	0 (0)	0 (0)
Clival	4 (4)	1 (3)	2 (7)	1 (3)	0.9030	9 (19)	3 (13)	4 (40)	2 (13)
Frontal	14 (14)	5 (14)	1 (3)	8 (25)	0.1800	7 (15)	1 (4)	2 (20)	4 (27)
Occipital	5 (5)	0 (0)	0 (0)	5 (16)	**0.0330**	2 (4)	2 (9)	0 (0)	0 (0)
Parietal	6 (5)	1 (3)	2 (7)	3 (9)	0.7290	1 (2)	0 (0)	0 (0)	1 (7)
Temporal	6 (6)	1 (3)	2 (7)	3 (9)	0.7290	0 (0)	0 (0)	0 (0)	0 (0)
Tentorial	1 (1)	1 (3)	0 (0)	0 (0)	0.4850	0 (0)	0 (0)	0 (0)	0 (0)
Intraventricular	2 (2)	0 (0)	0 (0)	2 (6)	0.1930	1 (2)	0 (0)	0 (0)	1 (7)
Cerebellum	2 (2)	0 (0)	2 (7)	0 (0)	0.1930	0 (0)	0 (0)	0 (0)	0 (0)
Spine	2 (2)	0 (0)	2 (7)	0 (0)	0.1930	1 (2)	0 (0)	1 (10)	0 (0)
WHO grade (%)									
Grade I	77 (79)	35 (100)	24 (80)	18 (56)	**0.0020**	39 (81)	23 (100)	8 (80)	8 (53)
Grade II	20 (21)	0 (0)	6 (20)	14 (44)		9 (19)	0 (0)	2 (20)	7 (47)
Median MIB1 index (range)	3.1 (0.5–40)	2.5 (0.5–18.5)	3.5 (0.5–31.5)	6.3 (1–40)	**0.0040**	2.6 (1–32.7)	2.2 (1–5.5)	5 (2.5–16.5)	8.2 (1–32.7)
Extent of resection (%)									
Gross total resection	76 (79)	25 (71)	27 (90)	24 (75)	0.4820	38 (79)	16 (70)	9 (90)	13 (87)
Subtotal resection	20 (21)	10 (29)	3 (10)	7 (22)		10 (21)	7 (30)	1 (10)	2 (13)
Unknown	1 (1)	0 (0)	0 (0)	1 (3)		0 (0)	0 (0)	0 (0)	0 (0)
Median follow-up, mo (range)	28 (0–91)	26 (8–86)	25 (1–83)	31 (0–91)	0.5720	11.5 (0–20)	5 (0–17)	3 (0–17)	4 (0–20)
Death (%)	1 (1)	0 (0)	0 (0)	1 (3)	0.3580	1 (2)	0 (0)	1 (11)	0 (0)

Note that this table does not include recurrences (*SI Appendix*, Table S1). Boldface type indicates $P < 0.05$.

Of note, 79% of type C tumors showed loss of both 1p and 22q. All of the WHO grade III tumors in our sample (which were all recurrences) show this double loss, but 2 of the patients had multiple resections of WHO grade II tumors. Our molecular classification, by contrast, placed all these patients' tumors, from original to last, in type C. Moreover, that our type C tumors, the most aggressive type, included all WHO grades underscores the importance of developing robust molecular profiles to supplement histopathology.

Our data suggest that testing for loss of even just these 2 chromosomes could provide a valuable biomarker for the risk of recurrence despite complete resection. In addition, it is worth noting that copy number variation alone may prove to be sufficient in distinguishing these 3 tumor types and certainly would be a simple test to carry out clinically. To solidify this correlation and its diagnostic value, future studies should evaluate these genomic loci in much larger samples.

The pressing need in the meningioma field is to understand the biology that differentiates aggressive meningiomas from less aggressive ones so that we may start dissecting the pathways that drive pathogenesis and establish the first step toward developing adjuvant therapies. Our 3 molecular types differ clinically and biologically and correlate with the clinical course better than the WHO classification. We continue to follow up on our patient population with the expectation that more data will yield further insight. Along similar lines, much larger cohorts will be needed to refine the molecular profiles (both genomic data and RNA expression) to a clinically translatable signature, to better understand meningioma biology and improve prognostication of the most difficult meningiomas.

Methods

Sample Selection and Preparation. We obtained 161 primary tumor tissue (fresh-frozen) samples from 141 patients who were treated at Baylor College of Medicine (BCM). All patients provided written informed consent, and tumor tissues were collected under an institutional review board (IRB)-approved protocol at BCM by the Human Tissue Acquisition and Pathology Core. All meningiomas were initially signed out by one of 2 neuropathologists (K.H. or J.C.G.) and were graded based on the 2016 WHO guidelines. MIB1 index was calculated by determining the percentage of meningioma cell nuclei positive for Ki-67 staining. We used blood DNA as a reference for detecting somatic tumor mutations. We performed RNA sequencing on 161 tumors. One tumor sample was noted to have a NAB2-STAT6 gene fusion that, based on the 2016 WHO guidelines (47), is now diagnostic for hemangiopericytoma/solitary fibrous tumor. Upon independent review by our neuropathologist, the patient was excluded from our analysis. We thus analyzed 160 meningiomas from 140

patients: 121 benign (WHO grade I), 32 atypical (WHO grade II), and 7 malignant (WHO grade III) meningiomas. One hundred twenty-eight of these samples had adequate DNA for WES. Only representative fresh-frozen blocks with estimated purity of ≥95% were selected for DNA and RNA extraction from 20 to 30 mg of tumor tissue using TRIzol (Thermo Fisher Scientific) according to the manufacturer's protocol. Normal DNA was extracted from 1 mL of whole blood stored in PAXgene blood DNA tubes using the PAXgene Blood DNA Extraction Kit (Qiagen) according to the manufacturer's protocol.

Patient Data and Characteristics. Under the aegis of a BCM IRB-approved protocol, we reviewed the following data: patient age at surgery, sex, race, tumor size, tumor location, preoperative embolization, extent of resection, histologic grade by WHO guidelines, MIB1 index, and presence of brain invasion. Diagnostic imaging was rereviewed to define tumor location, extent of resection, and presence/date of local recurrence. Local recurrence after gross total resection was defined as local development of any contrast enhancement on subsequent brain imaging. Local recurrence after subtotal resection was defined as measurable growth of residual tumor. Vital status of the patient was obtained from search of the electronic medical record. A summary of clinical information is available in Table 1.

The breakdown of patients and profiled recurrences is as follows: 126 patients had only 1 tumor (126 tumors); 5 patients had 2 distinct tumors (for a total of 10 tumors); 6 patients had 1 recurrent tumor (12 tumors); 1 patient had a recurrence with 2 separate tumor masses (3 tumors); 1 patient had 4 sequential recurrences (5 tumors); and 1 patient had 2 sequential recurrences, where the second recurrence produced 2 distinct masses (4 tumors). This yielded a total of 160 tumors (126 + 10 + 12 + 3 + 5 + 4).

To look at the data another way, the discovery cohort contained 97 tumors from 95 patients on whom we operated between 2011 and 2017, including 2 patients that had 2 primary tumors. The validation set contained 48 tumors from 47 patients on whom we operated between 2017 and 2018, including 1 patient with 2 primary tumors. Two patients had a primary tumor in the discovery set and had a second primary tumor that ended up in the validation set.

Antibodies. Western blot (overnight incubation with a 1:5,000 dilution): anti-EED (chicken, GTX14294; GeneTex), anti-SUZ12 (D39F6, rabbit, 3737S; Cell Signaling Technology), anti-vinculin (hVIN, mouse, V9131; MilliporeSigma), anti-FOXM1 (rabbit, GTX102126; GeneTex), anti-MYBL2 (rabbit, GTX77893; GeneTex), anti-RBL2 (D9T7M, rabbit, 13610; Cell Signaling Technology), anti–mouse-HRP (1:50:000, 715-035-150; Jackson ImmunoResearch Labs, RRID:AB_2340770), anti–rabbit-HRP (1:20,000, 170-5046; Bio-Rad/AbD Serotec, RRID:AB_11125757), and anti–chicken-HRP (1:2,000, NBP1-74785; Novus Biologicals). Coimmunoprecipitation: anti-EZH1 (rabbit, 2 μg per immunoprecipitation, GTX108013; GeneTex) and anti-LIN37 (rabbit, 5 μg per immunoprecipitation, GTX44925; GeneTex).

Coimmunoprecipitation. PRC2 immunoprecipitations were carried out with 10 mg of tissue in 200 μL of PRC2 lysis buffer (50 mM Hepes, pH 7.0, 250 mM NaCl, 0.1% Nonidet P-40, 5 mM EDTA, freshly added: 0.5 mM DTT, 1 mM PMSF, 1× Xpert Phosphatase Inhibitor, and 1× Xpert Protease Inhibitor Mixture [P3200 and P3100, GenDEPOT]). DREAM immunoprecipitations were carried out with 50 mg of tissue in 200 μL of DREAM lysis buffer (20 mM Tris, pH 7.5, 420 mM NaCl, 1.5 mM MgCl2, 1 mM EDTA, 5% glycerol, freshly added: 1 mM DTT, 1 mM PMSF, 1× Xpert Phosphatase Inhibitor, and 1× Xpert Protease Inhibitor Mixture). After tissue disruption via sonication (3 rounds with 3, 4, and 5 pulses, respectively, at 20% duty cycle), lysates were cleared via centrifugation for 20 min at 21,000 rcf at 4 °C and transferred to siliconized tubes. The antibody was added, and after a 2-h incubation at 4 °C on a rotor 40 μL of agarose beads were added for another 30 min. Antibody–bead complexes were washed 5 times in their respective buffers and subject to standard Western blot analysis using 1% input and 50% eluates.

Cell Culture and qRT-PCR. Arachnoid cells were immortalized using a lentivirus harboring the SV40 large T antigen; pBABE-puro SV40 LT was a gift from Thomas Roberts, Dana-Farber Cancer Institute, Boston, MA (Addgene RRID:Addgene_13970) as previously described (48). NF2 haplotype was validated using qRT-PCR using a dilution series of DNA from 293T (NF2 wild type) and arachnoid cells. The 293T cell line was purchased from ATCC (CRL-3216). Cells were found to be negative for mycoplasma contamination. Cell lines were cultured as adherent cells in DMEM containing 10% FBS and antibiotics using standard cell culture practices. The 293T or arachnoid cells were transfected using Lipofectamine 3000 (Thermo Fischer) using the following constructs: hEZH1-GFPpcDNA3 (amino acids 1 through 747), EZH1_deltaSET-GFPpcDNA3 (amino acids 1 through 512), hLIN37-GFPpcDNA3 (amino acids 1 through 243), hLIN37_CD1/2-GFPpcDNA3 (amino acids 1 through 243) (41), hLIN52-GFPpcDNA3 (1 through 116), and Lin52_S28A-GFPpcDNA3 (42). After 48 h of culture, total RNA was isolated using TRIzol, subject to reverse transcription and qRT-PCR.

ACKNOWLEDGMENTS. We thank the patients, without whom this study would not be possible. We thank Chad Shaw, PhD, for reviewing the paper to ensure proper bioinformatics/statistical methodology was used. Portions of this study were funded by the Roderick D. MacDonald Fund, the Jan and Dan Duncan Neurologic Research Institute at Texas Children's Hospital, and the Hamill Foundation. A.J.P. is supported by a K08 award from the National Institute of Neurological Disorders and Stroke (K08NS102474). H.Y.Z. is supported by the Howard Hughes Medical Institute. The Human Tissue Acquisition & Pathology Core at Baylor College of Medicine is funded through P30 Cancer Center Support Grant NCI-CA125123. We thank Vicky Brandt for insightful comments on the manuscript and Dima Suki for providing advice on statistical analysis.

1. Q. T. Ostrom *et al*., CBTRUS statistical report: Primary brain and central nervous system tumors diagnosed in the United States in 2008-2012. *Neuro Oncol.* **17** (suppl. 4), iv1–iv62 (2015).
2. J. Wiemels, M. Wrensch, E. B. Claus, Epidemiology and etiology of meningioma. *J. Neuro Oncol.* **99**, 307–314 (2010).
3. B. E. Pearson *et al*., Hitting a moving target: Evolution of a treatment paradigm for atypical meningiomas amid changing diagnostic criteria. *Neurosurg. Focus* **24**, E3 (2008).
4. M. K. Aghi *et al*., Long-term recurrence rates of atypical meningiomas after gross total resection with or without postoperative adjuvant radiation. *Neurosurgery* **64**, 56–60, discussion 60 (2009).
5. A. Modha, P. H. Gutin, Diagnosis and treatment of atypical and anaplastic meningiomas: A review. *Neurosurgery* **57**, 538–550, discussion 538–550 (2005).
6. A. Zaher, M. Abdelbari Mattar, D. H. Zayed, R. A. Ellatif, S. A. Ashamallah, Atypical meningioma: A study of prognostic factors. *World Neurosurg.* **80**, 549–553 (2013).
7. L. Rogers *et al*., Meningiomas: Knowledge base, treatment outcomes, and uncertainties. A RANO review. *J. Neurosurg.* **122**, 4–23 (2015).
8. R. G. W. Verhaak *et al*.; Cancer Genome Atlas Research Network, Integrated genomic analysis identifies clinically relevant subtypes of glioblastoma characterized by abnormalities in PDGFRA, IDH1, EGFR, and NF1. *Cancer Cell* **17**, 98–110 (2010).
9. C. G. A. R. Network; Cancer Genome Atlas Research Network, Integrated genomic analyses of ovarian carcinoma. *Nature* **474**, 609–615 (2011).
10. C. M. Perou *et al*., Molecular portraits of human breast tumours. *Nature* **406**, 747–752 (2000).
11. T. J. Pugh *et al*., Medulloblastoma exome sequencing uncovers subtype-specific somatic mutations. *Nature* **488**, 106–110 (2012).
12. M. Peyre, M. Kalamarides, Molecular genetics of meningiomas: Building the roadmap towards personalized therapy. *Neurochirurgie* **64**, 22–28 (2018).
13. A. S. Harmancı *et al*., Integrated genomic analyses of de novo pathways underlying atypical meningiomas. *Nat. Commun.* **8**, 14433 (2017).
14. F. Sahm *et al*., DNA methylation-based classification and grading system for meningioma: A multicentre, retrospective analysis. *Lancet Oncol.* **18**, 682–694 (2017).
15. V. E. Clark *et al*. Genomic analysis of non-NF2 meningiomas reveals mutations in TRAF7, KLF4, AKT1, and SMO. *Science* **339**, 1077–1080 (2013).
16. V. E. Clark *et al*., Recurrent somatic mutations in POLR2A define a distinct subset of meningiomas. *Nat. Genet.* **48**, 1253–1259 (2016).
17. P. K. Brastianos *et al*., Genomic sequencing of meningiomas identifies oncogenic SMO and AKT1 mutations. *Nat. Genet.* **45**, 285–289 (2013).
18. W. L. Bi *et al*., Genomic landscape of high-grade meningiomas. *NPJ Genom. Med.* **2**, 15 (2017).
19. H. N. Vasudevan *et al*., Comprehensive molecular profiling identifies FOXM1 as a key transcription factor for meningioma proliferation. *Cell Rep.* **22**, 3672–3683 (2018).
20. A. Olar *et al*., Global epigenetic profiling identifies methylation subgroups associated with recurrence-free survival in meningioma. *Acta Neuropathol.* **133**, 431–444 (2017).
21. F. Nassiri *et al*.; International Consortium on Meningiomas, DNA methylation profiling to predict recurrence risk in meningioma: Development and validation of a nomogram to optimize clinical management. *Neuro Oncol.*, 10.1093/neuonc/noz061 (2019).
22. A. J. Kane *et al*., Anatomic location is a risk factor for atypical and malignant meningiomas. *Cancer* **117**, 1272–1278 (2011).
23. H. Huang, Y. Liu, M. Yuan, J. S. Marron, Statistical significance of clustering using soft thresholding. *J. Comput. Graph. Stat.* **24**, 975–993 (2015).
24. A. Olar *et al*., Mitotic index is an independent predictor of recurrence-free survival in meningioma. *Brain Pathol.* **25**, 266–275 (2015).
25. Z. Swiderska *et al*., Comparison of the manual, semiautomatic, and automatic selection and leveling of hot spots in whole slide images for Ki-67 quantification in meningiomas. *Anal. Cell. Pathol. (Amst.)* **2015**, 498746 (2015).
26. T. Rezanko, A. K. Akkalp, M. Tunakan, A. A. Sari, MIB-1 counting methods in meningiomas and agreement among pathologists. *Anal. Quant. Cytol. Histol.* **30**, 47–52 (2008).
27. D. X. Cai *et al*., Chromosome 1p and 14q FISH analysis in clinicopathologic subsets of meningioma: Diagnostic and prognostic implications. *J. Neuropathol. Exp. Neurol.* **60**, 628–636 (2001).
28. P. Müller *et al*., Deletion of chromosome 1p and loss of expression of alkaline phosphatase indicate progression of meningiomas. *Clin. Cancer Res.* **5**, 3569–3577 (1999).

29. L. Stögbauer, W. Stummer, V. Senner, B. Brokinkel, Telomerase activity, TERT expression, hTERT promoter alterations, and alternative lengthening of the telomeres (ALT) in meningiomas–A systematic review. *Neurosurg. Rev.*, 10.1007/s10143-019-01087-3 (2019).
30. V. M. Lu *et al*., The prognostic significance of TERT promoter mutations in meningioma: A systematic review and meta-analysis. *J. Neuro Oncol.* **142**, 1–10 (2019).
31. T. A. Juratli *et al*., Intratumoral heterogeneity and *TERT* promoter mutations in progressive/higher-grade meningiomas. *Oncotarget* **8**, 109228–109237 (2017).
32. A. Subramanian *et al*., Gene set enrichment analysis: A knowledge-based approach for interpreting genome-wide expression profiles. *Proc. Natl. Acad. Sci. U.S.A.* **102**, 15545–15550 (2005).
33. V. K. Mootha *et al*., PGC-1α-responsive genes involved in oxidative phosphorylation are coordinately downregulated in human diabetes. *Nat. Genet.* **34**, 267–273 (2003).
34. S. Sadasivam, J. A. DeCaprio, The DREAM complex: Master coordinator of cell cycle-dependent gene expression. *Nat. Rev. Cancer* **13**, 585–595 (2013).
35. M. von Schimmelmann *et al*., Polycomb repressive complex 2 (PRC2) silences genes responsible for neurodegeneration. *Nat. Neurosci.* **19**, 1321–1330 (2016).
36. N. Soshnikova, D. Duboule, Epigenetic temporal control of mouse hox genes in vivo. *Science* **324**, 1321–1323 (2009).
37. Y. Liu *et al*., Histone lysine methyltransferase Ezh1 promotes TLR-triggered inflammatory cytokine production by suppressing Tollip. *J. Immunol.* **194**, 2838–2846 (2015).
38. K. J. Abel *et al*., Characterization of EZH1, a human homolog of Drosophila Enhancer of zeste near BRCA1. *Genomics* **37**, 161–171 (1996).
39. E. Ezhkova *et al*., EZH1 and EZH2 cogovern histone H3K27 trimethylation and are essential for hair follicle homeostasis and wound repair. *Genes Dev.* **25**, 485–498 (2011).
40. I. Ben-Porath *et al*., An embryonic stem cell-like gene expression signature in poorly differentiated aggressive human tumors. *Nat. Genet.* **40**, 499–507 (2008).
41. C. F. Mages, A. Wintsche, S. H. Bernhart, G. A. Müller, The DREAM complex through its subunit Lin37 cooperates with Rb to initiate quiescence. *eLife* **6**, e26876 (2017).
42. L. Litovchick, L. A. Florens, S. K. Swanson, M. P. Washburn, J. A. DeCaprio, DYRK1A protein kinase promotes quiescence and senescence through DREAM complex assembly. *Genes Dev.* **25**, 801–813 (2011).
43. M. Fischer, P. Grossmann, M. Padi, J. A. DeCaprio, Integration of TP53, DREAM, MMB-FOXM1 and RB-E2F target gene analyses identifies cell cycle gene regulatory networks. *Nucleic Acids Res.* **44**, 6070–6086 (2016).
44. G. Collord *et al*., An integrated genomic analysis of anaplastic meningioma identifies prognostic molecular signatures. *Sci. Rep.* **8**, 13537 (2018).
45. A. Mosquera Orgueira, Hidden among the crowd: Differential DNA methylation-expression correlations in cancer occur at important oncogenic pathways. *Front. Genet.* **6**, 163 (2015).
46. H. Xiao, K. Bartoszek, P. Lio', Multi-omic analysis of signalling factors in inflammatory comorbidities. *BMC Bioinformatics* **19** (suppl. 15), 439 (2018).
47. D. N. Louis *et al*., The 2016 world health organization classification of tumors of the central nervous system: A summary. *Acta Neuropathol.* **131**, 803–820 (2016).
48. T. J. Klisch, A. Vainshtein, A. J. Patel, H. Y. Zoghbi, Jak2-mediated phosphorylation of Atoh1 is critical for medulloblastoma growth. *eLife* **6**, e31181 (2017).